

Flow-Inspired Lightweight Multi-Robot Real-Time Scheduling Planner

Han Liu¹, Yu Jin², Tianjiang Hu², and Kai Huang¹

Abstract—Collision avoidance and trajectory planning are crucial in multi-robot systems, particularly in environments with numerous obstacles. Although extensive research has been conducted in this field, the challenge of rapid traversal through such environments has not been fully addressed. This paper addresses this problem by proposing a novel real-time scheduling scheme designed to optimize the passage of multi-robot systems through complex, obstacle-rich maps. Inspired from network flow optimization, our scheme decomposes the environment into a network structure, enabling the efficient allocation of robots to paths based on real-time congestion data. The proposed scheduling planner operates on top of existing collision avoidance algorithms, focusing on minimizing traversal time by balancing robot detours and waiting times. Our simulation results demonstrate the efficiency of the proposed scheme. Additionally, we validated its effectiveness through real world flight tests using ten quadrotors. This work contributes a lightweight, effective scheduling planner capable of meeting the real-time demands of multi-robot systems in obstacle-rich environments.

Code: <https://github.com/chengji253/FRSP>

I. INTRODUCTION

Swarm robotics holds significant potential for various real-world applications, including air traffic control, search and rescue missions, and target detection. Much research has focused on ensuring the smooth and safe navigation of swarm robots in obstacle-rich environments.

In obstacle-rich environments, the primary challenge for multi-robot navigation is effective trajectory planning. Methods such as the artificial potential field method [1] [2], velocity obstacle (VO) and its variants [3] [4] [5], on-demand collision avoidance [6], gradient-based local planning methods [7], and distributed model predictive control (DMPC) [8] have been proposed to address it. These approaches mainly focus on collision avoidance, reduce computational load, minimize deadlocks, and handle complex environments. However, few methods focus on enabling rapid traversal through these areas.

Achieving rapid passage of multi-robot systems through obstacle-rich areas requires maximizing the utilization of every available path. This concept is similar to network flow problems, which aim to maximize flow from source to sink in a network [9]. The core of network flow lies in optimizing network capacity utilization to enhance flow and speed. We observe that the idea from maximum flow problems can be applied to efficiently schedule multi-robot

systems, accelerating their traversal through obstacle-rich regions.

However, real-time and efficient scheduling of multi-robot systems in obstacle-rich environments poses significant challenges. Flow-based methods cannot be directly applied to multi-robot systems for several reasons. First, flow-based methods require a predefined network structure, but real-world map environments often lack such readily usable network structures. Second, these methods typically have long computation times and are often designed for offline use, lacking real-time applicability. Additionally, flow-based methods do not account for robot collision avoidance and motion models. In scenarios with a large number of robots, collision avoidance becomes a primary cause of congestion. At this point, robots face a decision: either wait in congested areas or choose a longer but uncongested path. Therefore, a new scheduling scheme is required, one that can determine in real time which robots should wait and which should reroute, while also specifying alternative routes. Moreover, the scheduling process needs to allocate the number of robots based on path capacity to reduce congestion.

To address these challenges, we propose a real-time scheduling scheme for multi-robot systems. Our planner builds on existing collision avoidance algorithms. It does not directly solve robot collision avoidance but performs real-time scheduling based on the map environment and robot status. The scheduling scheme first decomposes the initial map and extracts information to form a network containing nodes, edges, and capacity information. Subsequently, the planner calculates the path for each robot in real-time based on the current position of the robots and the congestion level of the map channels. The planner optimizes path selection from the perspective of the entire swarm, balancing detouring and waiting to minimize the time required for robots to traverse obstacle-rich environments. Experimental results show that when the number of robots reaches 500, the calculation time per instance of our planner is only 0.9 seconds, demonstrating high computational efficiency. And we conducted flight tests to demonstrate that the proposed scheme can be applied to real-world settings.

Our contributions can be summarized as follows:

- We propose a novel scheduling planner that utilizes the traversable areas of the map, thereby reducing the traversal time for a swarm of robots in obstacle-rich environments.
- Our scheduling planner is lightweight and exhibits high computational efficiency, meeting the real-time requirements of the robots.
- We have validated the effectiveness of our algorithm

¹H. Liu and K. Huang are with the School of Computer Science, Sun Yat-sen University, Guangzhou, China.

²Y. Jin and T. Hu are with the School of Aeronautics and Astronautics, Sun Yat-sen University, ShenZhen, China.

E-mail: liuh386@mail2.sysu.edu.cn, huangk36@mail.sysu.edu.cn

through extensive experiments.

II. RELATED WORK

Many methods have been developed to address the navigation challenges of multiple robots in obstacle-rich environments, each with a distinct focus. The artificial potential field method is often favored for its low computational load and high scalability [1], [2]. Velocity obstacle (VO) based methods and their variants have shown good performance in multi-robot navigation scenarios [3], [4], [5]. Optimization-based approaches, including on-demand collision avoidance [6], gradient-based local planning [7], and distributed model predictive control (DMPC) [8] aim to reduce computational time. Alonso-Mora *et al.* [10] introduced a planning method for multi-robot task execution in dynamic environments, ensuring task specification compliance and collision avoidance. Tordesillas *et al.* [11] proposed a decentralized and asynchronous trajectory planner that offers faster, safer, and more efficient navigation. Park *et al.* [12] presented a trajectory planning algorithm that uses dynamic linear safety corridors to construct feasible collision constraints, enabling deadlock-free planning in extreme environments. While these studies primarily focus on collision avoidance, reducing computational load, and managing complex scenarios, there is limited research on minimizing traversal time for multi-robot systems in obstacle-rich environments.

Since the pioneering research of Ford and Fulkerson on the maximum flow problem in networks [9], this field has attracted considerable attention. Variants such as the multi-commodity flow problem share similarities with multi-robot navigation challenges. The multi-commodity flow problem aims to transport a set of commodities from sources to destinations while respecting network capacity constraints and minimizing overall transportation cost or time. Trivella *et al.* [13] proposed an algorithm that balances delays and costs using penalty functions, enhancing the flexibility and cost efficiency of liner shipping networks. Bevrani *et al.* [14] introduced a multi-criteria multi-commodity network flow model to evaluate the resilience and vulnerability of transportation systems. Huang *et al.* [15] proposed a game-theoretic model and algorithm to optimize the decision-making process of multiple vehicles in a network. Khanal *et al.* [16] addressed the maximum static and dynamic multicommodity flow problem with intermediate storage. These methods generally require prior knowledge of network information and focus on adhering to capacity limits or reducing transportation costs. Their computational time is often lengthy, making them unsuitable for direct application in multi-robot navigation.

III. PROBLEM STATEMENT

We consider a 2-dimensional workspace $\mathcal{W} \subseteq \mathbb{R}^2$ and a set of M static obstacles $\mathcal{O} = \{o_1, \dots, o_M\}$ with $o_i \subset \mathcal{W}$. There are N robots indexed by $n \in \{1, 2, \dots, N\} = \mathcal{N}$ who need to pass through the environment. Each robot n has a start location $\mathbf{s}^{(n)} \in \mathcal{W}$ and a goal location $\mathbf{g}^{(n)} \in \mathcal{W}$. The robots are modeled as unit masses in \mathbb{R}^2 , with single

integrator dynamics. We use $\mathbf{p}^{(n)}(t), \mathbf{v}^{(n)}(t)$ to represent the discretized position, velocity at time step t of the n th robot. With a discretization step h , the dynamic equations are given by

$$\mathbf{p}^{(n)}(t+h) = \mathbf{p}^{(n)}(t) + h\mathbf{v}^{(n)}(t) \quad (1)$$

We constrain the motion of the robots to match the physics of the vehicle. The robots have limited actuation, which bounds its maximum velocity: $\|\mathbf{v}^{(n)}(t)\| \leq \mathbf{v}_{\max}$. The collision avoidance constraint is designed such that the robots safely traverse the environment:

$$\|\mathbf{p}^{(i)}(t) - \mathbf{p}^{(j)}(t)\| \geq r_{\min}, \quad i, j \in \mathcal{N}, i \neq j \quad (2)$$

$$\|\mathbf{p}^{(i)}(t) - o_j\| \geq r_{\min}, \quad i \in \mathcal{N}, o_j \in \mathcal{O}. \quad (3)$$

The Eqs.(2), (3) show that the distance between any two robots and the distance between robots and obstacles must be higher than the minimum safety distance r_{\min} .

To fulfill the mission requirements, robots must navigate from starting points, traverse an obstacle-rich environment, and ultimately reach their destinations. During this process, robots must account for collision avoidance both among themselves and with the obstacles. The efficiency of the overall traversal of multi-robot system is measured by the time taken for the last robot to reach the destination. In scenarios where path capacity is limited and the number of robots is large, collision avoidance can lead to congestion, thereby decreasing the overall traversal efficiency.

To address this issue, we need to consider: (1) How to allocate the number of robots based on path capacity to reduce congestion. (2) When facing congestion ahead, whether a robot should wait or reroute, and if rerouting, which path to select. (3) How to make decisions between a shorter but congested path and a longer but clear path. As our scheme focuses on scheduling, we will adopt existing solutions for collision avoidance algorithms. In the experimental section, we will employ the Reciprocal Velocity Obstacles (RVO) algorithm [3] for collision avoidance.

IV. NETWORK CONSTRUCTION

In this section, we delve into the details of network construction. The initial map is typically a grid map containing information on obstacles and traversable areas. To construct the subsequent network, we first decompose the map using the Boustrophedon Cellular Decomposition method [17]. This method scans the map by moving back and forth, similar to the way oxen plow fields, dividing the map into multiple cells. Denote the cell set containing all cells as \mathcal{C} . Next, we will introduce how to construct “PathNode” and “PathPos” at the boundary position of the cells.

A. “PathNode” and “PathPos”

We extract the length and positional information of each boundary of cells and establish passage positions at the shared boundaries of adjacent cells. Denote the shared boundary length as L_B . Then, the number of passage positions that can be established on the boundary is $\frac{L_B}{\alpha r_{\min}}$,

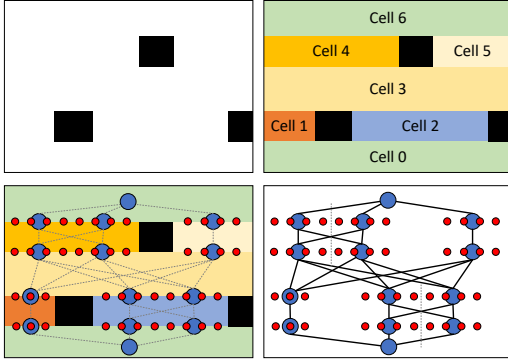


Fig. 1: The network construction process. The blue circles represent the “PathNode” of the network, and the red circles represent the “PathPos” of each node.

where α is a constant. Typically α is set to $1 \sim 2$, to ensure sufficient maneuvering space for the robots. The number of passage positions represents the capacity of boundary, which is the maximum number of robots that can pass through simultaneously. These passage positions are defined as “PathPos” (red circles in Fig.(1)). Next, we group every N_B passage positions together, partitioning the red positions into multiple groups. Then, we place a new node at the mean position of each group. The new node is defined as “PathNode” (blue circles in Fig.(1)). If the remaining number of red positions is less than N_B , they form a separate group. “PathNode” and “PathPos” serve as bridges between the actual map and the network graph for the robots.

After establishing the nodes, we create links between the nodes on the upper and lower boundaries of a cell. The nodes on the lower boundary of a cell are connected to all nodes on the upper boundary, ultimately forming a complete network. Define the capacity of node i as $\text{Cap}(i)$, which is the number of passage positions of this node. Denote the network as a graph $\mathcal{G} = \{\mathcal{V}, \mathcal{L}\}$ that includes a set of nodes \mathcal{V} and a set of links \mathcal{L} . Each link $l = (i, j) \in \mathcal{L}$ has its corresponding length $\text{Len}(l)$. The start of link $\text{START}(l) = i$, the end node of link $\text{END}(l) = j$. Let $\text{UP}(c) \subset \mathcal{V}$ represent the upper boundary node set of cell c , $\text{DN}(c) \subset \mathcal{V}$ represent the lower boundary node set of cell c . Define a function $\text{Dijkstra}(i, j)$ to find the dijkstra shortest path with a start node of i and an end node of j . It will return a path node list connecting nodes i and j . Denote the start cell and goal cell of robot n as $c_{star}^{(n)}, c_{goal}^{(n)}$. Define the capacity of link l as $\text{Cap}(l)$:

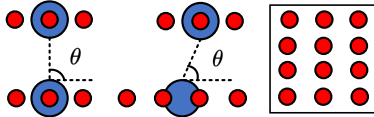


Fig. 2: The capacity of link

$$\text{Cap}(l) = \frac{\text{Len}(l) \sin(\theta)}{\alpha r_{\min}} \min(\text{Cap}(i), \text{Cap}(j)) \quad (4)$$

where $i = \text{START}(l), j = \text{END}(l)$. θ is the angle between the link l and the horizontal direction (Fig.(2)). The capacity of l is the minimum capacity of its two endpoints, multiplied by the projection of the length of l in the vertical direction, and then divided by αr_{\min} . $\text{Cap}(l)$ can be interpreted as the maximum number of robots that can be accommodated on link l at one time.

B. State variable

After constructing the network, the next step is to define the state variables of the robots within the network. Let $c_{now}^{(n)}(t)$, $d_{pre}^{(n)}(t)$ and $d_{nex}^{(n)}(t)$ denote the current cell, previous node and target node of robot n at time t . The link connecting the previous node and the target node is denoted as $l^{(n)}(t)$, with $\text{START}(l^{(n)}(t)) = d_{pre}^{(n)}(t)$ and $\text{END}(l^{(n)}(t)) = d_{nex}^{(n)}(t)$. The $l^{(n)}(t)$ represents the link where the robot is currently at time t . Denote the total number of robots on link l as $\text{Num}(l)$. Then, the state variable of the robot can be represented as:

$$X^{(n)}(t) = \left(c_{now}^{(n)}(t), d_{pre}^{(n)}(t), d_{nex}^{(n)}(t), l^{(n)}(t) \right) \quad (5)$$

where $c_{now}^{(n)}(t) \in \mathcal{C}$, $d_{pre}^{(n)}(t) \in \mathcal{V}$, $d_{nex}^{(n)}(t) \in \mathcal{V}$, $l^{(n)}(t) \in \mathcal{L}$.

C. Control variable

In the network, the control variables for the robot n at time t are the path node list $\text{PathNode}^{(n)}(t)$ and the path position list $\text{PathPos}^{(n)}(t)$. The $\text{PathNode}^{(n)}(t)$ represents the nodes that the robot needs to pass through, while $\text{PathPos}^{(n)}(t)$ specifies the exact passage positions. During its movement, the robot progresses towards the first position in $\text{PathPos}^{(n)}(t)$. Upon reaching the vicinity of this position, the following updates are triggered: (1) The first elements of the lists $\text{PathNode}^{(n)}(t)$ and $\text{PathPos}^{(n)}(t)$ are removed, indicating that the corresponding node and position have been traversed. (2) The previous node $d_{pre}^{(n)}(t)$ is updated to the node just traversed, and the next target node $d_{nex}^{(n)}(t)$ is updated to the first node in $\text{PathNode}^{(n)}(t)$. (3) The robot selects the first position in the path position list $\text{PathPos}^{(n)}(t)$ as the new target position and moves towards it. (4) As a result of the updates to the states $d_{pre}^{(n)}(t)$ and $d_{nex}^{(n)}(t)$, the edge $l^{(n)}(t)$ associated with the robot is also updated accordingly. Additionally, as the robot moves, it refreshes the state of the cell it occupies, and upon entering a new cell, the state $c_{now}^{(n)}(t)$ is automatically refreshed.

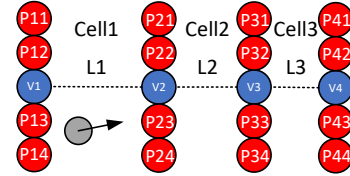


Fig. 3: State and control variables example

Fig.(3) illustrates an example of a robot navigating within a network. The network consists of four nodes (blue) and their corresponding positions (red). The current state variable

of the robot is $X^{(n)}(t) = (\text{Cell}_1, V_1, V_2, L_1)$, indicating that the robot is currently at Cell_1 , the previous node is V_1 , the goal node is V_2 , and the link is L_1 . At this point, the path nodes $\text{PathNode}^{(n)}(t) = [V_2, V_3, V_4]$, the path positions $\text{PathPos}^{(n)}(t) = [P_{23}, P_{33}, P_{42}]$, and $\text{Num}(L_1) = 1$. Upon reaching position P_{23} , the state of robot and control variables are updated. The new state variable becomes $X^{(n)}(t) = (\text{Cell}_2, V_2, V_3, L_2)$. Subsequently, the path nodes $\text{PathNode}^{(n)}(t) = [V_3, V_4]$, the path positions $\text{PathPos}^{(n)}(t) = [P_{33}, P_{42}]$, and $\text{Num}(L_2) = 1$.

V. SCHEDULING PLANNER

In this section, we discuss the details of our scheduling planner. As illustrated in Fig.(4), our scheduling planner consists of three main components: path set search, path node selection and local position allocation. The path node selection component calculates $\text{PathNode}^{(n)}(t)$ for each robot, while the local position allocation component determines the corresponding $\text{PathPos}^{(n)}(t)$. After these computations, the control variables are transmitted to the swarm robots, guiding them along their designated paths.

During movement, the robots continuously interact with the environment and with neighboring robots. In the presence of collision risks, the robots prioritize collision avoidance while following their paths. Both the scheduling planner and the collision avoidance algorithm operate in real-time, whereas the network construction is only required during the initial setup. Usually the frequency of the collision avoidance algorithm should be higher than the scheduling frequency.

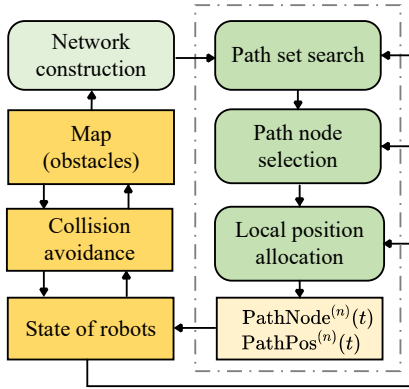


Fig. 4: The framework of our scheduling planner

A. Path set search

In scheduling planner, to identify a path from the start point to the destination, we first need to generate a set of potential paths. Given that the number of paths increases exponentially with the scale of the network, directly searching all possible paths would render the problem intractable. Considering the real-time requirements of robotic systems, the number of paths included in the set must be limited; otherwise, the subsequent computation time would be excessively long. Therefore, our search algorithm must

identify promising paths within a limited timeframe to facilitate subsequent optimization and selection.

Define the next-go-to path set for the n th robot as $\mathcal{P}_{\text{next}}^{(n)}(t)$, which represents the set of paths that the robot can potentially take from its current state in the future. During each decision-making instance, the robot considers only the paths within this set. The path search process is as follows: (1) Identify all PathNodes on the upper boundary of the cell where the robot is currently located $\text{UP}(c_{\text{now}}^{(n)}(t))$; (2) Identify all PathNodes on the lower boundary of the goal cell $\text{DN}(c_{\text{goal}}^{(n)})$; (3) Compute the paths from all upper boundary PathNodes to the lower boundary PathNodes using Dijkstra's algorithm. (4) Add the resulting paths to path set. The next-go-to path set $\mathcal{P}_{\text{next}}^{(n)}(t)$ can be written as:

$$\left\{ [\text{Dijkstra}(i, j)] \mid i \in \text{UP}(c_{\text{now}}^{(n)}(t)), j \in \text{DN}(c_{\text{goal}}^{(n)}) \right\} \quad (6)$$

Thus, we find the next-go-to path set for the n th robot. The rationale behind this method of computing the path set is that our algorithm is designed for real-time operation, rather than offline processing. Therefore, it is unnecessary to spend excessive time finding all possible intermediate paths. Instead, we only need to consider the viable paths from the robot's current state to the destination. Our experiments have demonstrated that this search method is highly efficient, with the time for a single search involving 500 robots being approximately 0.4 seconds, and the final decision-making performance is satisfactory.

B. Path node selection

After obtaining the result of $\mathcal{P}_{\text{next}}^{(n)}(t)$, the next step is to select a path from the set. The selected path result is assigned to $\text{PathNode}^{(n)}(t)$ as the control variable of the robot. In this section, we will introduce a method based on mixed-integer programming.

Denote p as a path element in the set $\mathcal{P}_{\text{next}}^{(n)}(t)$. Denote the decision variable as $z_p^{(n)}(t)$, which is a binary variable that represents whether the n th robot choose the path p at time t . Then the set of decision variables \mathcal{Z} is written as:

$$\mathcal{Z} = \left\{ z_p^{(n)}(t) \mid n \in \mathcal{N}, p \in \mathcal{P}_{\text{next}}^{(n)}(t) \right\} \quad (7)$$

The set \mathcal{Z} has decision variables of all robots. Since the robot can only choose one path at a time, we need to introduce the constraint,

$$\sum_{p \in \mathcal{P}_{\text{next}}^{(n)}(t)} z_p^{(n)}(t) = 1. \quad (8)$$

which means that the n th robot can only choose one path from the set $\mathcal{P}_{\text{next}}^{(n)}(t)$.

Denote the $\mathcal{P}_{\text{next}}(t)$ as the union of all sets $\mathcal{P}_{\text{next}}^{(n)}(t)$,

$$\mathcal{P}_{\text{next}}(t) = \bigcup \left\{ \mathcal{P}_{\text{next}}^{(n)}(t), n \in \mathcal{N} \right\} \quad (9)$$

Denote the first and second link of path p is $\text{Fir}(p)$ and $\text{Sec}(p)$. They are the link connecting the first node and the second node, and the link connecting the second node and the third node in the path p respectively. Denote the $\text{Fir}(\mathcal{P}_{\text{next}}(t))$

and $\text{Sec}(\mathcal{P}_{\text{next}}(t))$ as the set of first links and second links of path set $\mathcal{P}_{\text{next}}(t)$,

$$\text{Fir}(\mathcal{P}_{\text{next}}(t)) = \{\text{Fir}(p) \mid p \in \mathcal{P}_{\text{next}}(t)\} \subset \mathcal{L}, \quad (10)$$

$$\text{Sec}(\mathcal{P}_{\text{next}}(t)) = \{\text{Sec}(p) \mid p \in \mathcal{P}_{\text{next}}(t)\} \subset \mathcal{L}. \quad (11)$$

Denote $\mathcal{P}_{\text{fir}}^l(t)$ as the set of path that the first link of path p is l ,

$$\mathcal{P}_{\text{fir}}^l(t) = \{p \mid p \in \mathcal{P}_{\text{next}}(t), \text{Fir}(p) = l\}. \quad (12)$$

Denote $\mathcal{P}_{\text{sec}}^l(t)$ as the set of path that the second link of path p is l ,

$$\mathcal{P}_{\text{sec}}^l(t) = \{p \mid p \in \mathcal{P}_{\text{next}}(t), \text{Sec}(p) = l\}. \quad (13)$$

Introducing the definitions of these sets serves as the foundation for our subsequent introduction of queueing cost. We will analyze the potential for future congestion in robots based on whether all paths share the first and second links.

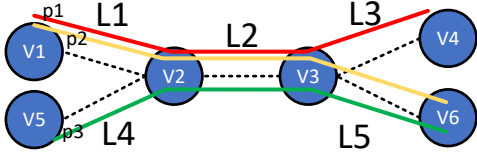


Fig. 5: An example of first and second link. The blue circles represent the “PathNode”. The red, orange and green lines represent three paths. The dotted line represents the link.

Fig.(5) shows an example of first link and second link. There are three paths $p_1 = [V_1, V_2, V_3, V_4]$ (red), $p_2 = [V_1, V_2, V_3, V_6]$ (orange), $p_3 = [V_5, V_2, V_3, V_6]$ (green). p_1, p_2 share links L_1, L_2 . p_2, p_3 share link L_2 . At this time, $\mathcal{P}_{\text{next}}(t) = \{p_1, p_2, p_3\}$. The first links of all paths have L_1, L_4 , the second link of all paths is L_2 . Thus, we have $\text{Fir}(\mathcal{P}_{\text{next}}(t)) = \{L_1, L_4\}$. $\text{Sec}(\mathcal{P}_{\text{next}}(t)) = \{L_2\}$. $\mathcal{P}_{\text{fir}}^l(t) = \{p_1, p_2\}, l = L_1$. $\mathcal{P}_{\text{fir}}^l(t) = \{p_3\}, l = L_4$. $\mathcal{P}_{\text{sec}}^l(t) = \{p_1, p_2, p_3\}, l = L_2$.

1) *Link queueing cost:* In this part, we will introduce how to calculate queueing cost through the first and second links. Define the queueing cost of the first link as $f_{\text{Fir}}(t)$:

$$\sum_{l \in \text{Fir}(\mathcal{P}_{\text{next}}(t))} \frac{\left(\sum_{n \in \mathcal{N}} \sum_{p \in \mathcal{P}_{\text{fir}}^l(t)} z_p^{(n)}(t) + \text{Num}(l) - \text{Cap}(l) \right)^2}{\text{Cap}(l)^2} \quad (14)$$

The term $\sum_{n \in \mathcal{N}} \sum_{p \in \mathcal{P}_{\text{fir}}^l(t)} z_p^{(n)}(t)$ represents the number of times link l is selected across all robots path results. When added to the current number of robots on link l , this gives the total number of robots on link l after decision-making. We then subtract the capacity of link l , and compute the square of the resulting value. This represents the queueing cost for the first link. Summing the queueing cost for all first links yields $f_{\text{Fir}}(t)$. This cost term ensures that the path node selection does not exceed the capacity of the links. When there are already many robots on an link, the remaining capacity is limited, and assigning more robots to that link will increase the loss. Similarly, if the sum of the assigned and existing

robots is less than the capacity, the loss will also increase, encouraging the decision-making process to fully utilize the link capacities.

Define the queueing cost of the second link as $f_{\text{Sec}}(t)$,

$$\sum_{l \in \text{Sec}(\mathcal{P}_{\text{next}}(t))} \frac{\left(\sum_{n \in \mathcal{N}} \sum_{p \in \mathcal{P}_{\text{sec}}^l(t)} z_p^{(n)}(t) + \text{Num}(l) - \text{Cap}(l) \right)^2}{\text{Cap}(l)^2} \quad (15)$$

The Equ.(15) is identical to the first link cost of Equ.(14). By incorporating the cost of the second link, the length of the paths considered in each planning step is extended, thereby imparting a degree of predictiveness to the decision-making process. Typically, the coefficient of $f_{\text{Sec}}(t)$ is smaller than $f_{\text{Fir}}(t)$, as the congestion in the map changes with the movement of robot. Therefore, the cost of the first link is prioritized.

2) *Running cost:* Running cost must also be considered. Each robot needs to balance between rerouting and waiting. Sometimes, the time cost of choosing a longer path may exceed the cost of waiting in place, necessitating a trade-off between the two. Therefore, a running cost penalty should be incorporated into the objective function to achieve more rational decision-making. Denote the running cost function as $f_{\text{run}}(t)$:

$$f_{\text{run}}(t) = \sum_{n \in \mathcal{N}} \sum_{p \in \mathcal{P}_{\text{next}}(t)} \text{Len}(p) z_p^{(n)}(t) \quad (16)$$

where $\text{Len}(p)$ is the length of path p . Putting these things together, a complete mixed-integer quadratic programming (MIQP) model is obtained, summarized below.

$$\text{minimize}_{z_p^{(n)}(t)} \quad k_1 f_{\text{Fir}}(t) + k_2 f_{\text{Sec}}(t) + k_3 f_{\text{run}}(t) \quad (17)$$

subject to: Eqs.(6), (8), (9), (10), (11), (12), (13). k_1, k_2, k_3 are weight coefficients. After this MIQP process, the specific binary values $z_p^{(n)}(t)$ can be obtained, which represent the path node selection result $\text{PathNode}^{(n)}(t)$.

C. Local position allocation

Upon obtaining the path node selection results $\text{PathNode}^{(n)}(t)$, the next step is to allocate specific node positions $\text{PathPos}^{(n)}(t)$ for the robots. Each node has multiple positions, and we utilize a greedy algorithm for this allocation. Initially, we select the position closest to the current position of robot. For each subsequent node, we select the position that is nearest to the previously allocated position. This process is repeated iteratively, ensuring each chosen position is the closest to the last assigned position. We employ a greedy algorithm instead of more complex alternatives. Our experiments show that the greedy algorithm is both simple and efficient, with the allocation time for 500 robots being approximately 0.02 seconds.

VI. EXPERIMENTS

This section provides an experimental analysis of our method. Our experiments are conducted on a PC with an Inter Core-i7 12700 CPU under 32GB of RAM. We

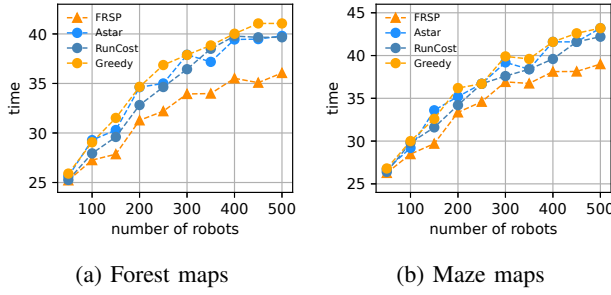


Fig. 6: Time results w.r.t. number of drones

compared the following methods to verify the performance of the proposed method:

- (1) Astar: Each robot uses the Astar algorithm to calculate the path from the starting point to the goal point.
- (2) Greedy: Find all paths from the upper boundary node of the starting cell to the lower boundary node of the goal cell. Then, use a greedy approach to evenly distribute robots across each path according to the path length and capacity.
- (3) RunCost: The method is almost the same as FRSP. But the objective function only has running cost. The coefficients are set to $k_1 = 0, k_2 = 0, k_3 = 1$.
- (4) FRSP: Our scheduling planner. The coefficients are set to $k_1 = 1, k_2 = 0.5, k_3 = 0.5$. The MIQP is solved by Gurobi [18].

The maps are categorized into two types: random forest and maze, with 5 maps generated for each type. For each map, we conducted experiments with varying numbers of robots, specifically: 10, 50, 100, 150, 200, 250, 300, 350, 400, 450, 500. The initial and goal positions of the robots are uniformly arranged in a matrix queue format. The parameters for the experiments are set as follows: $r_{\min} = 0.4m$, $\alpha = 2$, $h = 0.01s$, $v_{\max} = 3m/s$, $N_B = 4$. Our local collision avoidance algorithm utilizes the Reciprocal Velocity Obstacles (RVO) [3] method, chosen for two primary reasons. Firstly, RVO demonstrates reliable performance in multi-robot collision avoidance, reducing the likelihood of deadlocks. Secondly, it offers high computational efficiency, maintaining acceptable computation times even with a large number of robots. The frequency of collision avoidance algorithm is 100 Hz and the scheduling is 1 Hz.

Fig.6 shows the time results with respect to the number of robots in forest and maze maps. For every number of robots N , mean values are reported for each type of 5 maps. From the figures, we can make the following observations: (1) When N is small, there is not much difference between the time of four methods. This is because when the number is small, congestion rarely occurs, so the time results of the methods are similar. (2) As N increase, the time results increase. The gap between time results of FRSP and other methods is gradually increasing. This is because as N increases, the congestion starts to worsen, and the robots will waste more time waiting. FRSP can plan new paths for the waiting robots, thus reducing the time it takes to cross. The larger N is, the better FRSP works. (3) FRSP performs

		The average improvement		
		Astar	RunCost	Greedy
FRSP	Forest	8.66%	7.52%	10.77%
	Maze	6.58%	4.68%	7.54%

TABLE I: The average improvement of FRSP

	Average computation time (unit: seconds)						
Number	10	50	100	200	300	400	500
Path set search	0.050	0.076	0.105	0.158	0.262	0.326	0.456
Path node selection	0.014	0.058	0.114	0.181	0.243	0.317	0.447
Position allocation	0.000	0.002	0.004	0.008	0.015	0.013	0.025
Sum	0.064	0.136	0.223	0.347	0.520	0.656	0.928

TABLE II: The average computation time of FRSP

better on forest maps than on maze maps. This is because the forest map is more complex than the maze map, and there are more forks in the network structure. This shows that FRSP can adapt to complex map structures, and the more complex the map structure, the better the effect.

Table.I shows the average improvement of FRSP. The improvement ratio of FRSP in forest map compared with the other three methods are 8.66%, 7.52%, 10.77%. The improvement ratio of FRSP in maze map are 6.58%, 4.68%, 7.54%. It can be seen that the Greedy method is not as good as RunCost and Astar. This is because both RunCost and the Astar choose the shortest distance path, and they will wait when faced with congestion. But Greedy assigns robots to each path according to the greedy idea. Although congestion was reduced, time was wasted on further travel, suggesting that sometimes waiting may be a good option. Table.II shows the computation time with respect to the number of robots N . It can be seen that: (1) Path set search and path node selection take up most of the computation time, while local position allocation takes very little computation time. (2) When N is 10, the computation time of FRSP is about 0.06 seconds. When N is 500, the computation time of FRSP is about 0.9 seconds. This shows that our FRSP is computationally efficient and meets the real-time requirements.

A. Real World Flight Test

We conduct flight tests with ten DJI Tello drones within a forest environment. The drones are constrained to a space of $15m \times 5m \times 2m$ to prevent them from completely circumventing obstacle areas. All computations are performed on a single laptop. The supplementary video demonstrates the complete execution of the test, with no collisions or deadlocks occurring throughout the flight.

VII. CONCLUSION

In this paper, we proposed a flow inspired scheduling planner to optimize the traversal of multi-robot systems through obstacle-rich environments. Simulation and experimental results demonstrate the effectiveness of our scheduling planner.

REFERENCES

- [1] A. K. Pamosoaji and K.-S. Hong, "A path-planning algorithm using vector potential functions in triangular regions," *IEEE Transactions on Systems, Man, and Cybernetics: Systems*, vol. 43, no. 4, pp. 832–842, 2013.
- [2] S. Hosseini Semnani, A. H. J. de Ruiter, and H. H. T. Liu, "Force-based algorithm for motion planning of large agent," *IEEE Transactions on Cybernetics*, vol. 52, no. 1, pp. 654–665, 2022.
- [3] J. Van den Berg, M. Lin, and D. Manocha, "Reciprocal velocity obstacles for real-time multi-agent navigation," in *IEEE international conference on robotics and automation (ICRA)*, 2008, pp. 1928–1935.
- [4] J. Snape, J. v. d. Berg, S. J. Guy, and D. Manocha, "The hybrid reciprocal velocity obstacle," *IEEE Transactions on Robotics*, vol. 27, no. 4, pp. 696–706, 2011.
- [5] J. Alonso-Mora, A. Breitenmoser, M. Ruffi, P. Beardsley, and R. Siegwart, "Optimal reciprocal collision avoidance for multiple non-holonomic robots," in *Distributed autonomous robotic systems: The 10th international symposium*. Springer, 2013, pp. 203–216.
- [6] C. E. Luis, M. Vukosavljev, and A. P. Schoellig, "Online trajectory generation with distributed model predictive control for multi-robot motion planning," *IEEE Robotics and Automation Letters*, vol. 5, no. 2, pp. 604–611, 2020.
- [7] X. Zhou, J. Zhu, H. Zhou, C. Xu, and F. Gao, "Ego-swarm: A fully autonomous and decentralized quadrotor swarm system in cluttered environments," in *2021 IEEE International Conference on Robotics and Automation (ICRA)*, 2021, pp. 4101–4107.
- [8] E. Soria, F. Schiano, and D. Floreano, "Predictive control of aerial swarms in cluttered environments," *Nature Machine Intelligence*, vol. 3, no. 6, pp. 545–554, 2021.
- [9] L. R. Ford Jr and D. R. Fulkerson, "Constructing maximal dynamic flows from static flows," *Operations research*, vol. 6, no. 3, pp. 419–433, 1958.
- [10] J. Alonso-Mora, J. A. DeCastro, V. Raman, D. Rus, and H. Kress-Gazit, "Reactive mission and motion planning with deadlock resolution avoiding dynamic obstacles," *Autonomous Robots*, vol. 42, pp. 801–824, 2018.
- [11] J. Tordesillas and J. P. How, "Mader: Trajectory planner in multiagent and dynamic environments," *IEEE Transactions on Robotics*, vol. 38, no. 1, pp. 463–476, 2021.
- [12] J. Park, Y. Lee, I. Jang, and H. J. Kim, "Dlsc: Distributed multi-agent trajectory planning in maze-like dynamic environments using linear safe corridor," *IEEE Transactions on Robotics*, 2023.
- [13] A. Trivella, F. Corman, D. F. Koza, and D. Pisinger, "The multi-commodity network flow problem with soft transit time constraints: Application to liner shipping," *Transportation Research Part E: Logistics and Transportation Review*, vol. 150, p. 102342, 2021.
- [14] B. Bevrani, R. Burdett, A. Bhaskar, and P. K. Yarlagadda, "A multi-criteria multi-commodity flow model for analysing transportation networks," *Operations Research Perspectives*, vol. 7, p. 100159, 2020.
- [15] K. Huang, X. Chen, X. Di, and Q. Du, "Dynamic driving and routing games for autonomous vehicles on networks: A mean field game approach," *Transportation Research Part C: Emerging Technologies*, vol. 128, p. 103189, 2021.
- [16] D. P. Khanal, U. Pyakurel, and T. N. Dhamala, "Maximum multi-commodity flow with intermediate storage," *Mathematical Problems in Engineering*, vol. 2021, no. 1, p. 5063207, 2021.
- [17] H. Choset, "Coverage of known spaces: The boustrophedon cellular decomposition," *Autonomous Robots*, vol. 9, pp. 247–253, 2000.
- [18] G. Optimization, *Gurobi Optimizer Reference Manual*, 2021. [Online]. Available: <https://www.gurobi.com/documentation/>